Applied Catalysis B: Environmental 186 (2016) 19–29

Contents lists available at ScienceDirect

Applied Catalysis B: Environmental

journal homepage: www.elsevier.com/locate/apcatb

In situ synthesis of In_2S_3@MIL-125(Ti) core–shell microparticle for the removal of tetracycline from wastewater by integrated adsorption and visible-light-driven photocatalysis

Hou Wang[a,b], Xingzhong Yuan[a,b,c,*], Yan Wu[d], Guangming Zeng[a,b], Haoran Dong[a,b], Xiaohong Chen[c], Lijian Leng[a,b], Zhibin Wu[a,b], Lijuan Peng[e]

[a] College of Environmental Science and Engineering, Hunan University, Changsha 410082, PR China
[b] Key Laboratory of Environment Biology and Pollution Control, Hunan University, Ministry of Education, Changsha 410082, PR China
[c] Collaborative Innovation Center of Resource–Conserving & Environment-friendly Society and Ecological Civilization, Changsha 410083, PR China
[d] College of Environment and Energy, South China University of Technology, Guangzhou 510006, PR China
[e] Guangzhou Institute of Geochemistry, Chinese Academy of Sciences, Guangzhou, 510006, PR China

ARTICLE INFO

Article history:
Received 3 October 2015
Received in revised form
21 December 2015
Accepted 23 December 2015
Available online 29 December 2015

Keywords:
Metal-organic frameworks
Indium sulfide
Adsorption
Photocatalysis
Tetracycline

ABSTRACT

Metal-organic frameworks (MOFs) have been attracted considerable attention in the field of energy generation and environmental remediation. In this article, a novel core–shell In_2S_3@MIL-125(Ti) (MLS) photocatalytic adsorbent was successfully prepared by a facile solvothermal method. The as-obtained materials were characterized by scanning electron microscopy, transmission electron microscopy, X-ray diffraction, N_2 adsorption–desorption isotherm, X-ray photoelectron spectroscopy, UV–vis diffuse reflection spectroscopy and zeta potentials. It is indicated that the hybrids consisted of MIL-125(Ti) as the core and three-dimensional In_2S_3 sheets network as the shell has high surface area, mesoporous structure, and improved electronegativity and visible-light absorption. The MLS exhibited excellent adsorption performance for the removal of tetracycline (TC) from water. The adsorption process is sensitive to the solution pH, ionic strength and initial TC concentration. The Langmuir isotherm and pseudo-second-order mode could well describe the adsorption process and adsorption kinetics. The adsorption mechanism is mainly responsible for surface complexation, π–π interactions, hydrogen bonding and electrostatic interactions. Further, in TC degradation experiments under visible light exposure in presence of core–shell MLS, the optimal additive content of MIL-125(Ti) in synthesis process was 0.1 g, and the corresponding photodegradation efficiency for TC was 63.3%, which was higher than that of pure In_2S_3 and pure MIL-125(Ti). The improved photocatalytic performance was mainly ascribed to the opened porous structure, effective transfer of photo-generated carriers, Ti^{3+}–Ti^{4+} intervalence electron transfer and the synergistic effect between MIL-125(Ti) and In_2S_3. The degradation by-products of TC molecules were monitored by three-dimensional excitation-emission matrix fluorescence spectroscopy. Parts of TC molecules were mineralized into CO_2 and H_2O. The core–shell MLS composites also revealed good performance for the removal of TC from real wastewater including medical wastewater, municipal wastewater and river water. Therefore, the novel hybrids may be used as promising photocatalytic adsorbent for wastewater purification.

1. Introduction

Persistent organic pollutants from industry or urban regions in the aquatic ecosystem are serious environmental issues because of their high toxicity, solubility, persistence and carcinogenicity [1,2]. For instance, antibiotics like tetracycline (TC), widely used in human health, animal husbandry and fish farming against infectious diseases, can induce the development of antibiotic-resistant pathogens and cause serious problems for human health and ecosystem balance when they enter into aqueous environments [3,4]. Antibiotic concentrations in raw domestic wastewater are usually reported in the range from 100 ng/L to 6 mg/L [5]. Therefore, an effective and economical technique needs to be urgently

* Corresponding author. Fax: +86 73188821413.
E-mail address: yxz@hnu.edu.cn (X. Yuan).

http://dx.doi.org/10.1016/j.apcatb.2015.12.041
0926-3373/

developed to remove antibiotic before releasing wastewater into the aquatic environment.

Various technologies have been reported to eliminate antibiotic, such as adsorption, microbial degradation, electrolysis, photocatalysis and membranes separation [6,7]. Among these methods, integrated adsorption and degradation are considered to be one of the most attractive and potential methods for organic pollution and heavy metal ions purification [8]. Semiconductor-based photocatalysis is considered as an effective technology for solving the current environmental problems with utilization of solar energy. The technology could degrade and mineralize organic pollutants into CO_2 and H_2O under mild condition. Integrated photocatalytic adsorbents such as activated carbon supported TiO_2 and hydrogentitanate nanofibres have high adsorption affinity and photocatalytic activity for organic pollutants removal [9,10]. However, TiO_2-based photocatalytic process suffers from some main technical barriers that limit its commercialization, i.e., the inefficient exploitation of visible light ($\lambda > 420$ nm), low adsorption capacity for hydrophobic pollutants, uniform distribution in aqueous suspension and difficult post-recovery of the TiO_2 particles after water treatment. An overview on limitations of TiO_2-based particles for photocatalytic degradation of organic pollutants had been reported by our groups [11]. Therefore, in order to enhance the properties of TiO_2-based photocatalysts for pollutant purification in real application, exploring novel TiO_2-based composites with strong absorbance for broad ranged visible lights, high efficiency and relatively large particles for easily reuse is emergently necessary.

Recently, significant progress about porous materials has been made due to their huge porosities, designable pore structures, and facile modification. Metal–organic frameworks (MOFs), consisting of organic linkers and metal-oxo clusters, have intriguing crystalline structures, tailorable chemistry, large specific surface area and well-defined porosity [12,13]. Consequently, much attention has been paid to potential applications of MOFs in gas capture and storage, chemical separation, sensor devices, drug delivery and catalysis [14–16]. Nevertheless, MOFs were not only served as adsorbents for the removal of acid gases and dye, but also considered as excellent photocatalysts in photocatalysis. For example, Vaesen et al. had demonstrated that the MIL-125(Ti)-NH_2 was a promising candidate for the capture of acid H_2S and CO_2 gases due to the presence of accessible —OH and —NH_2 sites together with the absence of Lewis acid sites and high adsorption values [17]. Guo et al. had also reported that pure MIL-125(Ti) could be an adsorbent for the removal of Rhodamine B from aqueous solution [18]. Dan-Hardi et al. had synthesized a photoactive titanium dicarboxylate (MIL-125(Ti) or $Ti_8O_8(OH)_4$—$(O_2C$—C_6H_4—$CO_2)_6$) and observed a reversible photochromic behavior induced by alcohol adsorption under ultraviolet irradiation [19]. The MIL-125(Ti), a crystalline titanium dicarboxylate with large surface area and accessible pore diameters, has thermal stability and excellent photochemical properties. This material can not only introduce high density of the immobilized Ti sites within porous structure, but also tune the photocatalytic properties via various modified technologies. Nevertheless, pure MIL-125(Ti) photocatalysts is only efficiency in ultraviolet light area and instability during photochemical operations in aqueous solution.

Recently, our groups had previously modified MIL-125(Ti) via using the 2-aminoterephthalicacid as organic link or graphitic carbon nitride as the supporter of MIL-125(Ti) grown [20,21]. It had indicated that these photocatalysts exhibited excellent photocatalytic activity for Cr(VI) reduction and dye mineralization in wastewater under the visible light irradiation. Metal sulfides, a major group of abundant and cheap minerals such as CdS, SnS_2, Sb_2S_3 and so on, have been demonstrated as visible photocatalysts for the removal of pollutants in aqueous solution [22]. Indium(III) sulfide (In_2S_3) with various morphologies including nanoplates, nanotubes, hollow microspheres and nanorods has attracted great attention due to its good photosensitivity and photoconductivity, stable chemical and physical characteristics and low toxicity [23]. For instance, Wei et al. synthesized flowerlike β-In_2S_3 microspheres with relatively high visible-light photocatalytic activity for the mineralization of methyl orange [24]. Zhou et al. obtained hierarchical Bi_2S_3/In_2S_3 core/shell microspheres with enhanced photocatalytic activity for the degradation of 2, 4-dichlorophenol under visible light irradiation [25]. Interestingly, the hierarchical porous flower-like shell of In_2S_3 remarkably enhanced the chemical stability of Bi_2S_3 against oxidation. However, to the best of our knowledge, there has been no report on the preparation and applications of core–shell In_2S_3@MIL-125(Ti) composite as integrated photocatalytic adsorbent for the removal of antibiotics in wastewater.

The present work quantitatively investigates the adsorption of antibiotics (e.g., tetracycline) on core–shell In_2S_3@MIL-125(Ti) hybrids. Effects of different ratio of MIL-125(Ti) to In_2S_3, pH, ion strength and initial concentration on removal of TC were carried out. The adsorption kinetic and isothermal was subsequently studied. Further, the photocatalytic performance, mechanism and reutilization of the composite for the removal of TC were also investigated for potential applications. At last, the IPA for the removal of various real water samples including medical wastewater, municipal wastewater and river water via the integrated adsorption and photocatalytic process were preliminary explored.

2. Experimental

2.1. Materials

Tetrabutyl titanate (TBT; $C_{16}H_{36}O_4Ti$), 1,4-benzenedicarboxylic acid (BDC; $C_8H_6O_4$), *N*′*N*-dimetylformanide (DMF; $(CH_3)_2NCHO$), methanol (CH_3OH), Indium Nitrate ($In(NO_3)_3{\cdot}xH_2O$), Carbon Disulfide (CS_2) and Thioacetamide (CH_3CSNH_2), were purchased from Sinopharm Chemical Reagent Co., Ltd. (Shanghai, China). All reagents and solvents were of analytical reagent grade and used as received from commercial suppliers. River water (the value of chemical oxygen demand is 12.6 mg/L) was taken from Xiangjiang River located in Changsha, Hunan province, China. Medical wastewater (the value of chemical oxygen demand is 458.6 mg/L) was obtained from a hospital in Changsha, Hunan province, China. Municipal wastewater (the value of chemical oxygen demand is 185.5 mg/L) was obtained from Yuelu sewage treatment plant in Changsha, Hunan province, China.

2.2. Synthesis of core–shell In_2S_3@MIL-125(Ti) composites

The pure MIL-125(Ti) was fabricated by the same method described in our previous reports [20]. For the preparation of In_2S_3/MIL-125(Ti) composites, a certain amount of MIL-125(Ti) powder was dispersed into ethanol absolute with the aid of ultrasonication. 1 mmol $In(NO_3)_3{\cdot}xH_2O$ and 2 mL CS_2 were dissolved into the MIL-125(Ti) dispersion. After 30 min, 1 mmol CH_3CSNH_2 was added and agitated until the CH_3CSNH_2 was absolutely dissolved. The mixture was subjected to solvothermal conditions in a Teflon-lined stainless-steel autoclave for 12 h at 150 °C. After reaction, the yellow precipitate was separated by centrifugation and washed with absolute ethanol. After drying in a vacuum at 60 °C, the final products were collected for the following characterization and experiments. In order to obtain various ratio of MIL-125(Ti) to In_2S_3, the additive mass of MIL-125(Ti) during the synthesis process was 0.1 g, 0.3 g, 0.5 g, and 0.7 g. The as-obtained hybrids were denoted as MLS-1, MLS-3, MLS-5 and MLS-7. For comparison purposes, con-

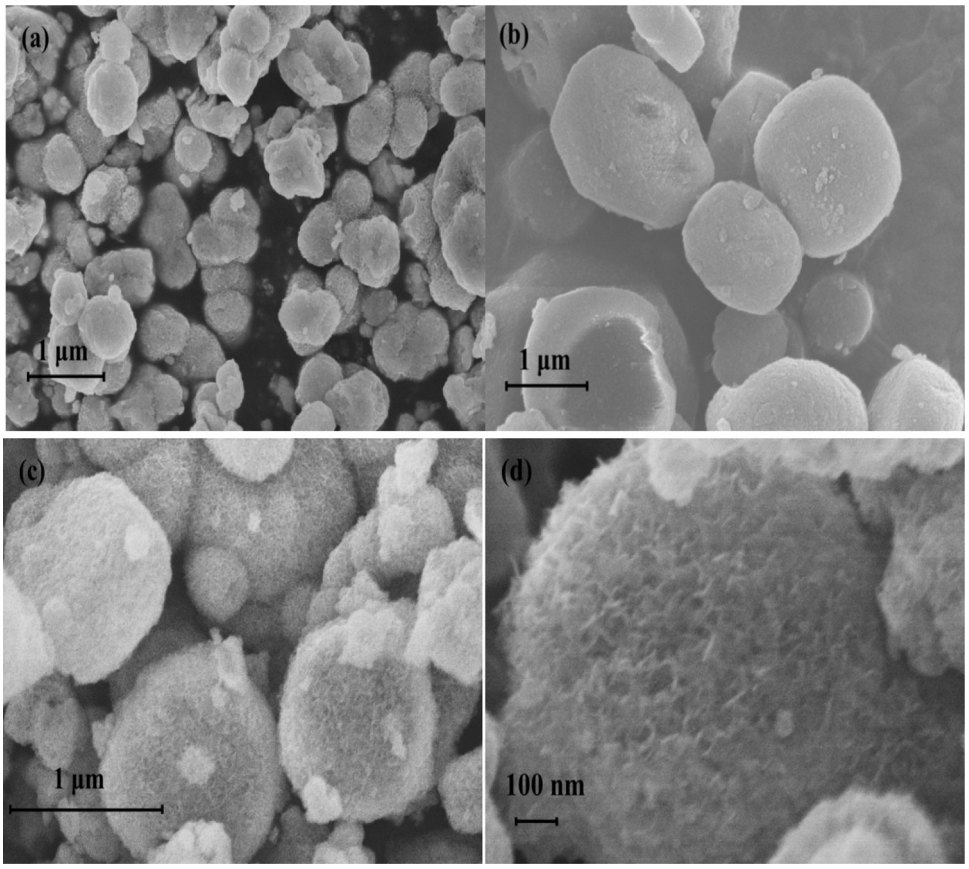

Fig. 1. SEM images of (a) pure In_2S_3, (b) pure MIL-125(Ti) and (c) MLS-5 sample. For comparison, higher magnification image (d) of MLS-5 composites is also shown.

ventional In_2S_3 was also prepared in the absence of MIL-125(Ti) under the same conditions.

2.3. Analytical methods

Bruker AXS D8 Advance diffractometer operating with Cu-K*a* source was used to record the powder X-ray diffraction (XRD). The morphologies of various samples were observed via scanning electron microscopy (SEM) (Hitachi S-4800, Japan) and transmission electron microscopy (TEM) (Tecnai G2 F20 S-Twin, USA). The chemical component and electronic state was investigated by X-ray photoelectron spectroscopy (Thermo Fisher Scientific, UK) [26]. The Brunauer–Emmett–Teller (BET) surface area was characterized by means of nitrogen absorption–desorption (ASAP2020, Micromeritics, USA). UV–vis diffuse-reflectance spectra (UV–vis DRS) were recorded in the range of 200–800 nm with a Varian Cary 300 spectrometer. The zeta potentials of as-prepared samples were determined as a function of pH (adjusted by 0.1 M HNO_3 or NaOH) using a Zeta-sizer Nano-ZS (Malvern, UK) [27]. Three-dimensional excitation-emission matrix fluorescence spectra (3D EMMs) were collected in the excitation wavelengths range of λ_{ex} = 200–450 nm and in the emission wavelengths range of λ_{em} = 300–550 nm (F-4500 spectrofluorimeter, Hitachi, Japan), and the detailed method was reported previously [28,29]. The total organic carbon (TOC) assays were carried out using a Shimadzu TOC-VCPH analyzer.

2.4. Adsorption experiments

Tetracycline (TC) was chosen as a typical antibiotic and the adsorption process was investigated by batch sorption experiments. Typically, tetracycline powder was dissolved in deionized water to prepare a stock solution of 100 mg/L concentration. All experimental TC solutions were prepared from the stock solution by dilution. The dark adsorption experiments were performed in 250 mL conical glass Erlenmeyer flasks containing 100 mL of the desired TC solution. The flasks were put into a dark room to prevent the illumination of slurries by ambient light. The homogeneity of suspensions was maintained by magnetic stirring. Samples were collected at designated time intervals, and analyzed by measuring absorbance at the maximum absorbance wavelength of TC using a Shimadzu UV–vis spectrophotometer at the wavelength of 357 nm.

2.4.1. Investigation of different influence factors

Four as-obtained MLS-1, MLS-3, MLS-5 and MLS-7 were selected to study the adsorption of TC molecules. For comparison, pure MIL-125(Ti) was also included. The pH of the solution may affect the surface charge of the composites, and consequently the adsorption of TC molecules. The experiment was conducted at the solution pH values of 3.3, 5.9, 7.2 and 9.5. The ionic strength of the solution was changed to study the effect on the adsorption process. In these experiments, sodium chloride (NaCl) was chosen and the concentration was 0.01, 0.05, 0.1 and 0.2 mol/L. Four TC concentrations (9.4, 28.7, 50.0 and 66.7 mg/L) were selected to study the kinetics of adsorption.

2.4.2. Adsorption kinetics and equilibrium

The amount of TC adsorbed at equilibrium was calculated from the following equation:

$$q_e = (C_i - C_e)\frac{V}{m}$$

where, C_i and C_e (mg/L) are the initial and equilibrium concentration of TC in solution, V (L) is the solution volume and m (g) is the mass of the composites. Adsorption kinetics and equilibrium

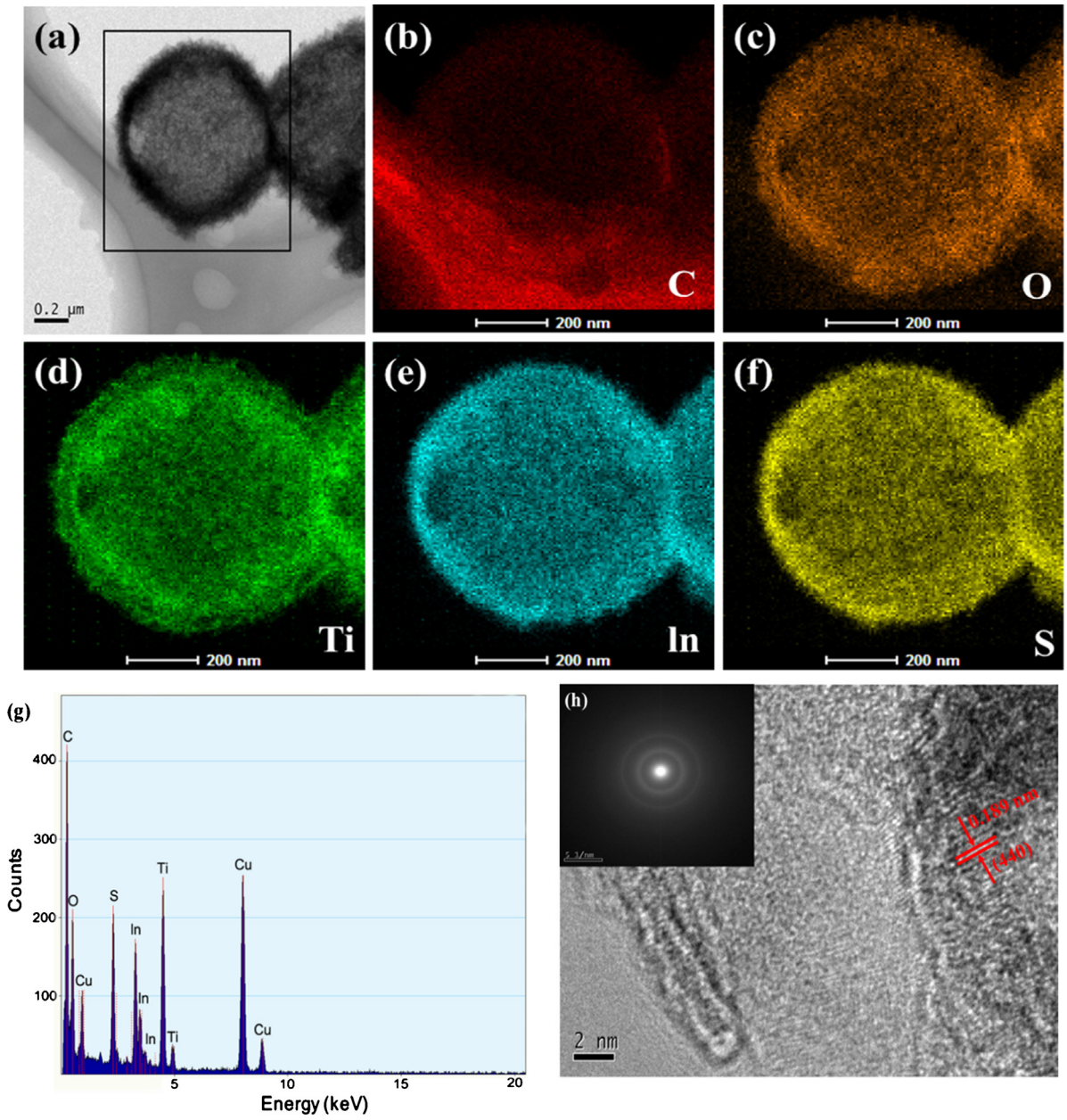

Fig. 2. (a) TEM image of MLS-5 sample and TEM mapping of the portion selected: (b) C, (c) O, (d) Ti, (e) In and (f) S; The (g) EDS analysis and (h) HRTEM images; The inset is the selected area electron diffraction pattern.

data were fitted to various models. The related equation has been listed Table S1 in Supporting Information according to our previous reports [27,30].

2.5. Photocatalytic experiment

Photocatalytic activity of core–shell In_2S_3@MIL-125(Ti) composites were tested by the photocatalytic decomposition of TC with visible light illumination ($\lambda > 420$ nm) after adsorption process. A 300 W Xenon lamp (CEL-HXF300, Beijing CEL Tech. Co., Ltd.) with a 420 nm cutoff filter was used as the visible light source (14 V, 16 A, 15 cm far away from the photocatalytic reactor). The light intensity of 300 W Xenon lamp was 300 mW cm^{-2}. For decomposition of TC, 30 mg of photocatalyst was dispersed in 100 mL of 46 mg L^{-1} TC aqueous solution. Prior to irradiation, the suspension was magnetically stirred in the dark for 60 min to get adsorption–desorption equilibrium between photocatalyst and TC. At certain time intervals, samples were collected via filtrating by 0.22 μm PTFE syringe filters. The TC concentration before and after photo-degradation were monitored with a UV–vis spectrophotometer (UV-2250, SHIMADZU Corporation, Japan). The TC concentration after adsorption equilibrium is acted as the initial concentration (C_0). Additionally, the recycle experiments were also carried out three consecutive cycles to test the durability and recyclability. After each cycle, the photocatalyst was filtrated and washed for three times to remove residual impurities, and then dried at 60 °C for the next test.

3. Results and discussion

3.1. Characteristics of obtained samples

The surface morphology of pure In_2S_3, pure MIL-125(Ti) and MLS-5 measured by SEM is shown in Fig. 1(a–d). It is found that only irregular microparticles with particle sizes of 400–650 nm forms in

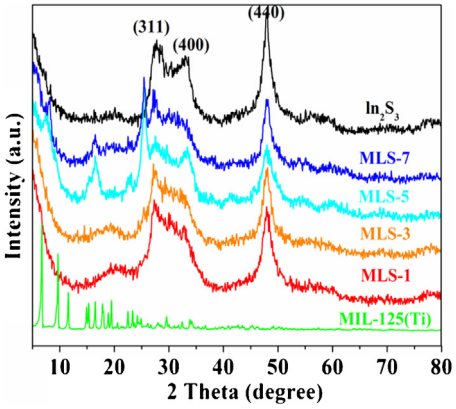

Fig. 3. XRD patterns of pure In_2S_3, pure MIL-125(Ti) and MLS samples.

the absence of MIL-125(Ti). MIL-125(Ti) has a plate-like form and smooth surface without secondary nanostructures. After solvothermal reaction at 150 °C in the presence of sulfur source and indium ions, the surface of MIL-125(Ti) becomes rough and the products still remain the original structures. The higher magnification SEM image (Fig. 1d) indicates a large number of In_2S_3 nanosheets grown onto the surface of MIL-125(Ti) are interconnected with each other, forming the three-dimensional (3D) nanosheets networks as a stable protective shell. The formation of uniform heterostructures may originate from the special characteristics of the MIL-125(Ti), i.e., the large surface area and porous structure, which facilitate the assembly of In_2S_3 nanosheets. This unique and ordered core–shell structured microparticle with 3D networks provides an abundant porous surface area for the contact between the materials and pollutants, which is of great significance in accelerating the adsorptive and photocatalytic reaction.

The typical TEM image of an individual MLS-5 microparticle is shown in Fig. 2a. The plate-like MIL-125(Ti) with the diameter of 800 nm is coated by a narrow size distribution of In_2S_3 nanosheets network automatically, indicating the formation of good quality In_2S_3@MIL-125(Ti) core–shell microparticle, which is well consistent with the SEM micrographs. From the energy dispersive spectrometer (EDS) mapping of the MLS-5 (Fig. 2e and f), it can be seen that the blue and yellow dots with bright color assigned to the In and S element, respectively, is uniformly distributed on the surface of In_2S_3@MIL-125(Ti) microparticle. For comparison, the C,O and Ti element mapping have also been shown in Fig. 2b–d. EDS spectrum (Fig. 2g) also displays the presence of In and S element in the core–shell microparticle, and the stoichiometric ratio of indium to sulphur is about 0.67, confirming successful fabrication of In_2S_3. The HRTEM image (Fig. 2h) of the heterostructures displays a clear lattice fringes with the nearest distance of 0.189 nm coinciding with the value for the (4 4 0) plane of cubic In_2S_3. The presence of the diffraction rings in the selected-area electron diffraction (SAED) pattern (inset of Fig. 2h) indicates that the cubic In_2S_3 nanosheets are polycrystalline. The crystalline structure of pure MIL-125(Ti), In_2S_3, and MLS were also examined by XRD, as shown in Fig. 3.

For the MLS with different weight addition of MIL-125(Ti), the XRD patterns are analogous to bare In_2S_3. The peaks located at $2\theta = 27.5°$, 33.4°, and 47.9° are distinctly indexed to the (3 1 1), (4 0 0) and (4 4 0) crystal planes of cubic In_2S_3 phase structure (β-In_2S_3) (JCPDS 32-0456) [23]. Meanwhile, compared to the XRD patterns of pure In_2S_3, some new peaks at 16.5° and 19.3° in MLS appear. The values of 2θ correspond to the characteristic peak of MIL-125(Ti), indicating the presence of MIL-125(Ti).

The chemical composition and valence state of various elements in the MLS-5 sample have been carried out by XPS measurement. The survey spectrum in Fig. 4a indicates that elements In, Ti, O, S and C exist in the MLS-5 sample while only the peaks of Ti, O and C appear in pure MIL-125(Ti). Fig. 4b shows the regional spectrum of In 3 d with two symmetrical peaks at the binding energy of In $3d_{5/2}$ (444.2 eV) and In $3d_{3/2}$ (451.7 eV). For the spectrum of S 2 p in Fig. 2c, the peaks at 160.7 eV and 161.8 eV are attributed to S $2p_{3/2}$ and S $2p_{1/2}$ transitions, respectively. The spin–orbit separations of In and S are found to be 7.5 eV and 1.1 eV, indicating that the In and S are present as $In^{3+}$and S^{2-} in the sample, respectively [25,26,31]. Fig. 4d shows Ti 2 p spectra of pure MIL-125(Ti) in comparison with that of the hybrids. The binding energy values of Ti $2p_{3/2}$ and Ti $2p_{1/2}$ at 459.2 and 464.9 eV, respectively, asserts the existence of Ti^{4+} for the titanium-oxo cluster [21]. However, a small shift toward lower binding energy is observed for MLS-5 as compared to pure MIL-125(Ti). This may be resulted from the higher ionization energy of sulfur in comparison with that of titanium [32]. The binding energy of 529.7 eV and 531.3 eV of O 1 s spectrum (Fig. 4e) may be ascribed to oxygen in titanium-oxo cluster and surface hydroxyl/ether groups. Meanwhile, in comparison with pure MIL-125(Ti), a negative shift of the O 1 s with an order of 0.8 eV is also observed for the MLS-5 sample. The shift order of O 1 s energy position is the almost same as that of the Ti 2 p peak position, implying the incorporation of sulfur in MIL-125(Ti) *via* S-Ti-O bond. These results are also the proofs for the formation of In_2S_3@MIL-125(Ti) core–shell heterostructures via chemical synthesis.

Table 1
Surface area, pore size and pore volume parameters for various materials.

Samples	Surface area[a] (m^2/g)	Pore size[b] (nm)	V_t[c] (cm^3/g)
MLS-1	303.9	3.732	0.464
MLS-3	287.4	3.709	0.440
MLS-5	253.9	3.710	0.393
MLS-7	208.6	3.713	0.659
MIL-125(Ti)	1548.3	3.833	0.758

[a] Measured using N_2 adsorption with the Brunauer–Emmett–Teller (BET) method.
[b] Pore size in diameter calculated by the desorption data using Barrett–Joyner–Halenda (BJH) method.
[c] Total pore volume determined at $P/P_0 = 0.99$.

The N_2 adsorption–desorption isotherms and the corresponding calculated parameters have shown in Fig. 5a and Table 1. The as-obtained samples are of type IV isotherm according to the IUPAC (International Union of Pure and Applied Chemistry) classification. Compared with pure MIL-125(Ti), MLS samples attain a decreased surface area and total pore volume (V_t). The phenomenon can be explained by the fact that a large amount of In_2S_3 nanosheets, grown on the surface of MIL-125(Ti), block the cavities or pores [21,22]. However, pore size with the diameter of 3.7–3.8 nm shows negligible change after the introduction of In_2S_3. Combining with the XRD results, it may be inferred that the current approach preserves the structural properties of MIL-125(Ti). The UV–vis absorption spectra were used to determinate the optical property of as-obtained samples. In Fig. 5b, pure In_2S_3 absorbs the light from the UV to visible-light, and its band gap absorption edge is around 600 nm, while no obvious absorption peak in the visible area is detected for MIL-125(Ti). As for MLS, a notable absorption extension in the visible-light region can be observed due to the In_2S_3 serving as the visible-light sensitizer. The absorption edges display a gradual blue-shift with increasing the addition amount of MIL-125(Ti) since the band gap of MIL-125(Ti) is wider than that of In_2S_3. According to the calculation of band gap energy in supporting information, the band gap energy (E_g) of In_2S_3 is 2.05 eV. As shown in Fig. S1, the band gap for MLS-1 is 2.28 eV, which is lower than that of pure MIL-125(Ti) (3.68 eV). Therefore, the formed heterojunction via the combination of In_2S_3 and MIL-125(Ti) provide an efficient utilization of visible light, thus producing more electron–hole pair. These results imply MLS are potential photocatalyst for the degradation of pollutants in wastewater under visible light irradiation.

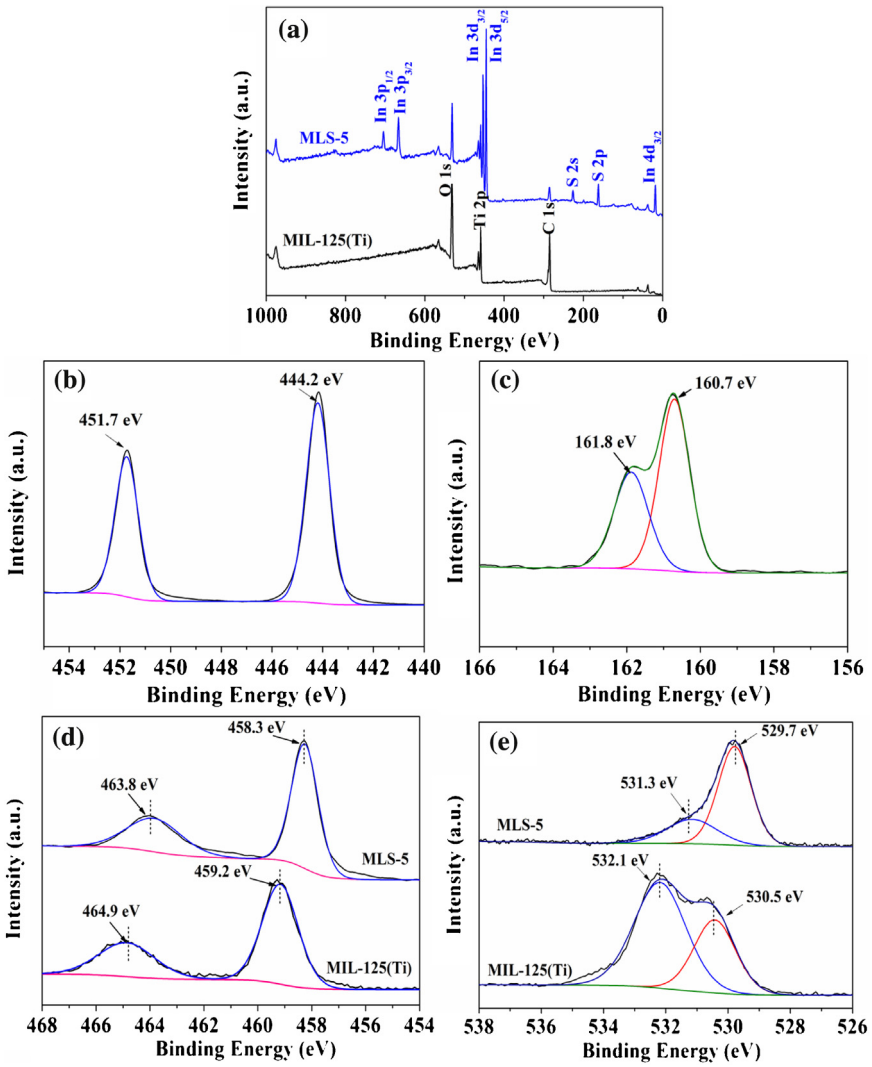

Fig. 4. The XPS spectra of MLS-5 sample: (a) survey scan, (b) In 3d, (c) S 2p, (d) Ti 2 p and (e) O 1 s; For comparison, the survey scan, Ti 2 p and O 1 s of pure MIL-125(Ti) sample are also shown.

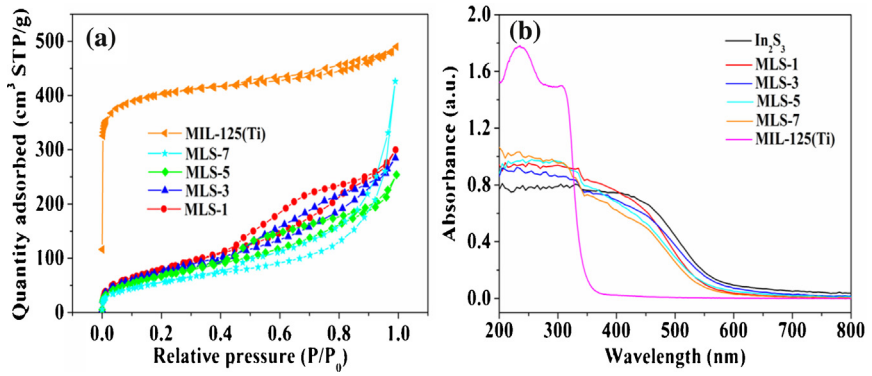

Fig. 5. (a) The N_2 adsorption-desorption isotherms of MIL-125(Ti), MLS-1, MLS-3, MLS-5 and MLS-7; (b) The UV–vis DRS of the as-obtained samples.

3.2. Effect of various conditions on TC adsorption

3.2.1. Different MLS for TC adsorption

TC adsorption of various MLS samples is investigated and the results are shown in Fig. 6a. Apparently, poor adsorption capacity (14.2 mg/g) has been obtained on the single MIL-125(Ti). An adsorption quantity of 84.9 mg/g is shown for pure In_2S_3. The MLS system exhibits enhanced adsorption performance and the adsorption capacity of TC increases initially with increasing MIL-125(Ti) mass, and then decreases as the mass further increases. The MLS-5 sample exhibits the highest adsorption performance and the adsorption amount of TC could be reach to 119.2 mg/g after 300 min. The improved performance may be due to that the presence of In_2S_3 enhances the complex interaction between the

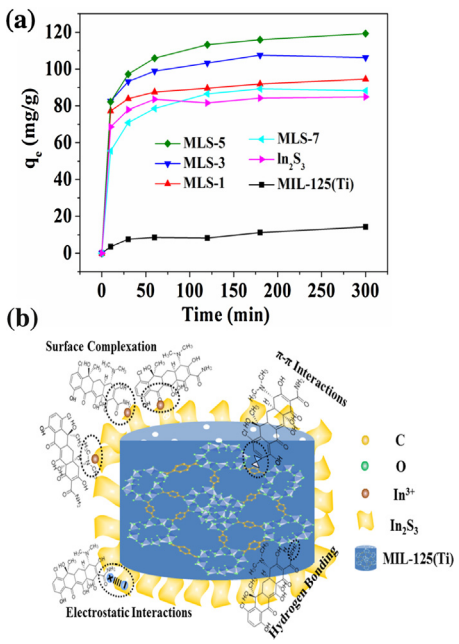

Fig. 6. (a) Adsorption performance of pure In_2S_3, MIL-125(Ti) and various MLS composites for TC removal. (Experimental conditions: initial TC concentration = 46 mg/L, pH 5.9, m = 30 mg, V = 100 mL). (b) The schematic illustration of adsorption mechanism.

exposed indium ions on In_2S_3 nanosheets surfaces and the polar functional groups of TC molecules [8]. In addition, the introduction of In_2S_3 nanosheets improves the electronegativity of MLS-5 compared to pure MIL-125(Ti) (as shown in Fig. S2), which is helpful for the removal of positively charged TC molecules. With the increase mass of MIL-125(Ti), the enhanced adsorption is due to the increased hydrogen bonding between the μ-OH groups (of the MIL-125(Ti)) and nitrogen atom of TC, and the π–π interaction between the organic link of MIL-125(Ti) and tetracycline molecules [17,33]. However, MLS-7 shows the lowest adsorption capacity, which may be the smaller specific surface area (Table 1) and the prominent effect of electrostatic repulsion between the positively charged MIL-125(Ti) and the positively charged TC molecules. The mechanism of TC adsorption onto MLS may be the synergistic effect of surface complexation, π–π interactions, hydrogen bonding and electrostatic interactions, as shown in Fig. 6b.

3.2.2. Effect of solution pH and ion strength

In practical applications, different water systems such as wastewater and surface water have various pH values. Tetracycline molecule is sensitive to the solution pH value because of its protonation state. In aqueous solutions, the groups of TC molecule, undergoing protonation–deprotonation reaction, can form three molecule species including cationic species (pH < 3.3), zwitterionic species(3.3 < pH < 7.68) or anionic species (pH > 7.68) [34,35]. For MLS, different pH has various physiochemical properties like surface charge, thus influencing the adsorptive interactions between the TC and the surface of MLS. Fig. 7a shows the effects of pH on the adsorption kinetics of TC on MLS-5. All curves have similar characteristics, showing an important and fast adsorption between t = 0 and 10 min, and a slower adsorption at longer time. Meanwhile, TC adsorption on the MLS-5 is strongly dependent on the solution pH values. The adsorption is relatively high at pH 3.3 and decreases significantly as the increased pH value from 5.9 to 9.5, indicating that the affinity of TC for the surface of MLS-5 is higher at low pH. As shown in Fig. S2, MLS-5 has an overall negative surface charge at pH 2.3–10.0. As the pH value increases, the zeta potentials are more negatively. At solution pH 9.5, both MLS-5 and anionic TC are negatively charged, and electrostatic repulsion may become a dominant interaction force, resulting in low adsorption. With the decrease of pH values in solution, an enhanced adsorption capacity can be explained by the predominant electrostatic attraction between opposite positively charged TC molecules and negatively charged MLS-5.

Different salts concentration involved in industrial wastewater may affect the TC removal. The effects of NaCl concentration on the TC adsorption onto MLS-5 at pH 3.3 are shown in Fig. 7b. Apparently, the adsorption depends on the ionic strength. It decreases significantly as the NaCl concentration increases from 0 to 0.1 mol/L and reach equilibrium from 0.1 to 0.2 mol/L. This phenomenon may be explained by the fact that the electrostatic protection, emerged after adding NaCl, restrains the immediate electrostatic interaction between positively charged TC (as TCH_3^+) and MLS-5. In addition, the competitive adsorption between TC molecules and Na^+ on the adsorptive sites of MLS-5 is enhanced with the increase of ionic strength [36].

3.3. Effect of initial TC concentration and kinetics studies

Fig. 8 shows the adsorption of TC onto MLS-5 using initial TC concentrations of 9.4, 28.7, 46.0 and 66.7 mg/L. It is evident that initial TC concentration plays a significant role in adsorption process, where 99.9%, 96.4%, 83.5% and 69.9% of TC are removed at the TC concentration equal to 9.4, 28.7, 46.0 and 66.7 mg/L, respec-

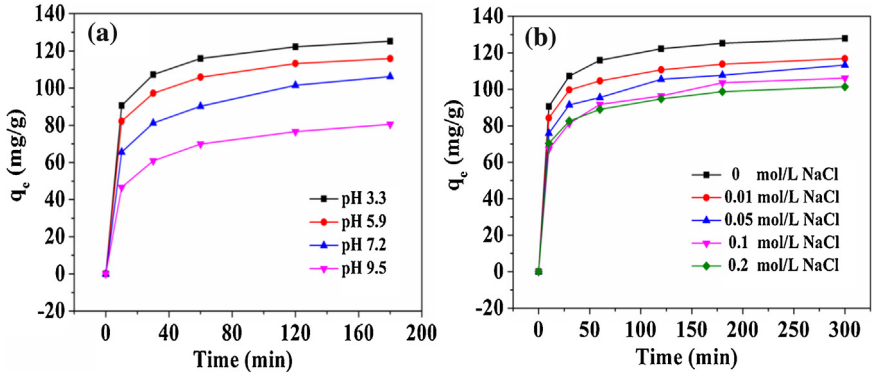

Fig. 7. Effect of (a) solution pH (Experimental conditions: initial TC concentration = 46 mg/L, m/V = 0.3 g/L, NaCl concentration = 0 mol/L), (b) NaCl concentration (Experimental conditions: initial TC concentration = 46 mg/L, m/V = 0.3 g/L, pH = 3.3), and (c) initial TC concentrations (Experimental conditions: m/V = 0.3 g/L, pH = 3.3, NaCl concentration = 0 mol/L) on the adsorption of TC onto MLS-5.

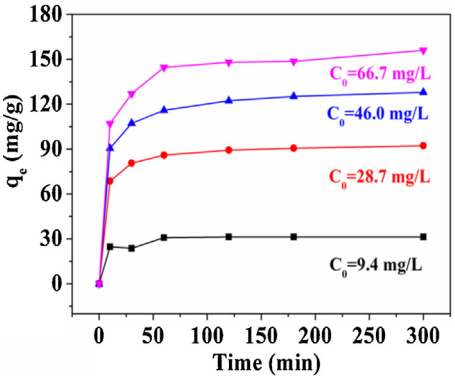

Fig. 8. Effect of different initial TC concentrations (Experimental conditions: m/V = 0.3 g/L, pH = 3.3, NaCl concentration = 0 mol/L) on the adsorption of TC onto MLS-5.

tively. The MLS-5 removes almost all the TC at relatively low initial concentration. In industrial application, high TC removal at low concentrations is considered to be of a great importance. The amount of TC adsorbed increases with the increase of time until the equilibrium is attained at 60 min for high TC concentrations (28.7, 46.0 and 66.7 mg/L), while almost all TC molecules are adsorbed within 10 min at 9.4 mg/L of TC. The initial uptake amount (first few minutes) for TC is relatively high since a large number of adsorption sites are available for adsorption. Later on, the adsorption decreases as the repulsive forces between the adsorbed TC molecules (on MLS-5) and the TC molecules in solution increases.

In order to analyze the process of TC adsorption onto MLS-5, the pseudo-first-order, pseudo-second-order, intra-particle diffusion and Boyd's film-diffusion model are examined at four different initial TC concentrations. Linear regressions of the kinetic plots are shown in Fig. S3. The kinetic parameters and calculated adsorption rate are listed in Table S2. Based on the correlation coefficients (R^2), the experimental data are best described by the pseudo-second-order model, which gives higher correlation coefficient values ($R^2 > 0.999$). What's more, the calculated q values ($q_{e,cal}$) calculated from the pseudo-second-order model are closer to the experimental q_e values ($q_{e,exp}$) than that calculated pseudo-first-order model. These results imply that the adsorption rate is probably controlled by chemisorption [37].

Further, the diffusion of TC molecules into the pores of MLS-5 has been determined via the intra-particle diffusion model. As can be seen from Fig. S3c, all plots are distributed in three linear segments presenting three different stages. The first stage is ascribed to external mass transfer diffusion of TC across the liquid film to the external surface of MLS-5, which is also called boundary layer diffusion of adsorbate molecules. The second stage describes the gradual adsorption, where the intra-particle diffusion is the rate-limiting step due to the pores or capillaries of the MLS-5 internal structure. The third stage is assigned to TC molecules adsorption onto the actives sites on the inner and outer surface of the MLS-5. The intra-particle diffusion starts to slow down because of the low concentration of TC remaining in solution and the insufficient actives sites. Furthermore, the second and third stages do not pass through the origin, indicating that intra-particle diffusion is not governed by the sole rate-limiting step [36]. Therefore, the overall adsorption process of TC onto MLS-5 may be resulted from both intra-particle diffusion and outer diffusion. To gain insights into the actual rate-controlling step, Boyd's model has been applied for distinguishing between outer diffusion and intra-particle diffusion control mechanisms. The linearity of the plot has been shown in Fig. S3d. Apparently, the regression lines do not pass through the origin, demonstrating the involvement of outer diffusion. Therefore, the overall adsorption process is jointly controlled by outer diffusion and intra-particle diffusion.

3.4. Adsorption equilibrium

The adsorption isotherm is crucial in providing useful information to understand the adsorption process and to design the adsorption system. Therefore, the experiment about the amount of TC adsorbed at equilibrium to MLS-5 at various TC concentrations has been carried out and the results have been depicted in Fig. S4a. Three typical adsorption models (Langmuir, Freundlich and Temkin models) are used to fit the experimental equilibrium adsorption data. The fitting results are shown in Fig. S4(b–d), and the calculated parameters are listed in Table S3. Experimental data fits Langmuir model much better than Freundlich and Temkin model, suggesting that the uptake of TC onto MLS-5 should be monolayer molecular adsorption process. Based on Langmuir model, the maximum adsorption capacity of TC on MLS-5 is calculated as 157.2 mg/g. Another essential characteristic of Langmuir isotherm, a dimensionless constant separation factor (R_L), can be expressed by the following equation:

$$R_L = \frac{1}{1 + k_L C_1}$$

where C_1 is the highest initial TC concentration (mg/L). This parameter indicates that the isotherm is unfavorable ($R_L > 1$), favorable ($R_L < 1$), linear ($R_L = 1$), or irreversible ($R_L = 0$) [38]. Calculated parameter (R_L) for TC adsorption on MLS-5 is 0.01, indicating that adsorption process is favorable at operation condition. The low R_L value (<0.04) demonstrates that the interaction between TC and MLS-5 is relatively strong [10].

3.5. Photocatalytic removal of TC

To prove the photocatalytic activity of obtained MLS as integrated photocatalytic adsorbent, photodegradation experiments of TC have been carried out under visible light illumination ($\lambda > 420$ nm) after adsorption process. According to the above batch adsorption experiments, suspension solution has been magnetically stirred in the dark for 60 min to establish adsorption/desorption equilibrium of TC onto MLS. The C/C_0 is applied to describe the degradation process (C and C_0 are the TC concentration at time t and 0, respectively). As shown in Fig. 9a , the TC could hardly be degraded without any photocatalyst, while MLS show much higher activity than that of pure In_2S_3 and MIL-125(Ti) under the visible light exposure. It is clearly indicated that the synergistic effect between MIL-125(Ti) and In_2S_3 as obtained by chemical synthesis. The highest photocatalytic activity is shown by MLS-1 with 63.3% of TC removal after 60 min of visible light irradiation. What's more, the photocatalytic activity of MLS decreases with the increase of the content of MIL-125(Ti). Increasing the content of MIL-125(Ti) will not only reduce the visible light absorption due to its large band gap, but also decrease the efficient heterointerfaces area between MIL-125(Ti) and In_2S_3. Moreover, when the amount of In_2S_3 is relatively low, the increased recombination of excited holes and electrons occurs, resulting in low photocatalytic efficiency [25].

Considering the fact that the amount of In_2S_3 in MLS is much smaller than pure In_2S_3 during the photocatalytic experiments, the heterostructure of MLS is the crucial influence in photocatalytic system process. On the one hand, the introduction of MIL-125(Ti) can provide extra surface area to improve the adsorption of TC molecules in the liquid phase. The opened mesoporous channels will not only make the active surface highly accessible to the TC molecules, but also improve the mass transfer within the hybrid structure during photocatalytic process. On the other hand, the

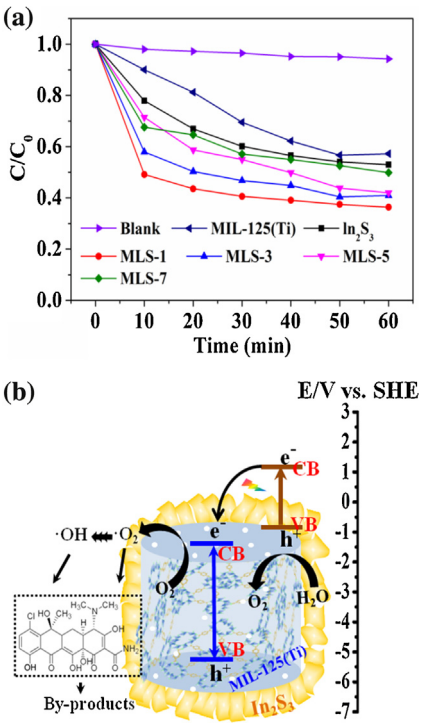

Fig. 9. (a) Photocatalytic performance of In_2S_3, MIL-125(Ti) and MLS for TC degradation. (Experimental conditions: initial TC concentration = 46 mg/L, pH 5.9, m = 30 mg, V = 100 mL) For comparison, photocatalytic performance for no photocatalyst is also given. (b) Schematic illustration of photo-generated charge carrier's separation and transfer in core–shell MLS sample.

heterostructures formation of MLS via the S—Ti—O bond leads to an effective transfer of the photo-generated carriers during the photocatalytic reaction. High surface-to-volume ratios facilitate the efficient transfer of electrons and holes to the surface of MLS.

3.6. Photocatalytic mechanism

Under visible light illumination, In_2S_3 with narrow band gap energy can be easily excited for the generation of electrons (e^-) and holes (h^+). The photo-generated electrons originated from In_2S_3 transfer to the Ti^{4+} in the titanium-oxo cluster of MIL-125(Ti) via the heterojunction structure, resulting in the reduction of Ti^{4+} to Ti^{3+}. Oxygen molecules in solution adsorbed onto porous MIL-125(Ti) form superoxide radicals ($^{\bullet}O_2^-$) via electron transfer from Ti^{3+} to O_2 due to the strong reducing ability of Ti^{3+} (−1.37 V vs SHE). The Ti^{3+} ions are oxidized and further convert to Ti^{4+} ions. The electrons transportation via the presence of Ti^{3+}–Ti^{4+} intervalence electron transfer had been demonstrated by Fu et al. [39]. and Wang et al. [20]. The relationship between the valence band (VB) and conduction band (VB) of MIL-125(Ti) and In_2S_3 in composite has been shown in Fig. 9b. For MIL-125(Ti), the CB above Fermi energy are mostly made up of Ti 3d, while the VB is mainly contributed from the O 2 p states mixed with a small amount of C 2 p states [40]. The photogenerated electrons transfer from the CB of In_2S_3 nanosheets to the CB of MIL-125(Ti) while the corresponding holes are left in the VB of In_2S_3 nanosheets to oxidize water into $O_{2(VB)}$. Then, the dissolved O_2 in solution as well as the $O_{2(VB)}$ capture the photogenerated electrons to yield $^{\bullet}O_2^-$ and subsequently produce $^{\bullet}OH$. The formed reactive species ($^{\bullet}OH$ and $^{\bullet}O_2^-$) efficiently degrade TC into other products. The main oxidative species produced in the photocatalytic process have also been demonstrated through radical and hole trapping experiments (as shown in Fig. S5) using EDTA-2Na (h^+ scavenger), p-benzoquinone ($^{\bullet}O_2^-$ scavenger), isopropyl alcohol ($^{\bullet}OH$ scavengers) or N_2 flow (excluding O_2) [41]. The results could also well support the proposed photocatalytic mechanism in Fig. 9b.

3D EMMs has been applied to characterize the residue solution after adsorption and photodegradation process. Four samples (M1–M4) were collected: M1, which was collected without adsorption and irradiation. M2 was taken after 60 min adsorption in the dark. M3 was taken after an irradiation time of 10 min. M4 was taken after a longer irradiation time of 60 min. Fig. 10 shows the 3D EEMs contour plots of samples M1–M4. Fluorescence quenching effect in the presence of TC has been manifested broadly throughout the 3D EEMs [28,42]. Thus, no fluorescence signal is observed for the initial TC solution and the residue TC solution after 60 min adsorption, as shown in Fig. 10(a and b). It is also demonstrated that TC molecule has not been broken or degraded into other products during the adsorption process. Upon the visible light illumination, the general characteristics of the 3D EEM plots for M3 (Fig. 10c) and M4 (Fig. 10d) include two maxima peaks in the wavelength range under investigation. According to the previous research reported by Coble et al. [43]. and Valencia et al. [29], the peak A at $\lambda_{ex}/\lambda_{em}$ = (305–330 nm)/(430–450 nm) and the peak B at $\lambda_{ex}/\lambda_{em}$ = (240–250 nm)/(435–450 nm) may be ascribe to humic acids-like fluorescence region and fulvic acids-like fluorescence region, respectively. The peak A and B is mainly due to the degradation of TC molecules by MLS-1 under visible light irradiation. However, the formation mechanisms of humic acids-like or fulvic acids-like substances in the TC degradation process is still unclear and will be deeply studied in the future research.

Further, fluorescence parameters (including peak location, maximum intensity, and peak intensity) of the residue solution after 10 min and 60 min irradiation have been extracted from 3D EEMs, and are listed in Table S4. Apparently, the intensity of peak B is higher than that of peak A, indicating a higher content of fulvic acids-like organic matter. For peak A, the peak intensity increases from 731.9 to 844.1, suggesting the increased content of humic acids-like organic matter with the increase of irradiation. However, the decreased peak intensity for peak B has been obtained, implying that fulvic acids-like matter reduce and may even be mineralized into CO_2 and H_2O. Total organic carbon test has been carried out to detect the carbon element in solution at 10 min and 60 min irradiation over MLS-1. The result shows that after 60 min of irradiation, a mineralization rate of 16.9%TOC removal is obtained, which is higher than that of 10 min irradiation (9.2% TOC removal).

3.7. Photocatalyst recyclability

To investigate the recyclability of photocatalyst, the MLS-1 sample after photocatalytic reaction is gathered by centrifugation and reused in the next photocatalytic reaction for three times under the same conditions. As shown in Fig. 11, the MLS-1 sample displays good recyclability in terms of photocatalytic TC degradation during three reaction cycles. As a result, MLS-1 is stable and recyclable for the photocatalytic degradation of TC, which is important for its practical application.

3.8. Preliminary experiment about the application of real wastewater treatment

From a practical point of view, the composition of wastewater is extremely complex. There is a need to investigate the effect of various wastewater for the removal of TC using MLS-1 as the IPA. Thus, the water including medical wastewater (pH 7.03), municipal wastewater (pH 6.96) and river water (pH 7.26) were used as the solution for the preparation of 40 mg/L TC-obtained wastewater. After the adsorption and photocatalytic process, more than 81%, 83% and 85% of TC is removed by MLS-1 for TC-obtained medical wastewater, municipal wastewater and river water, respectively.

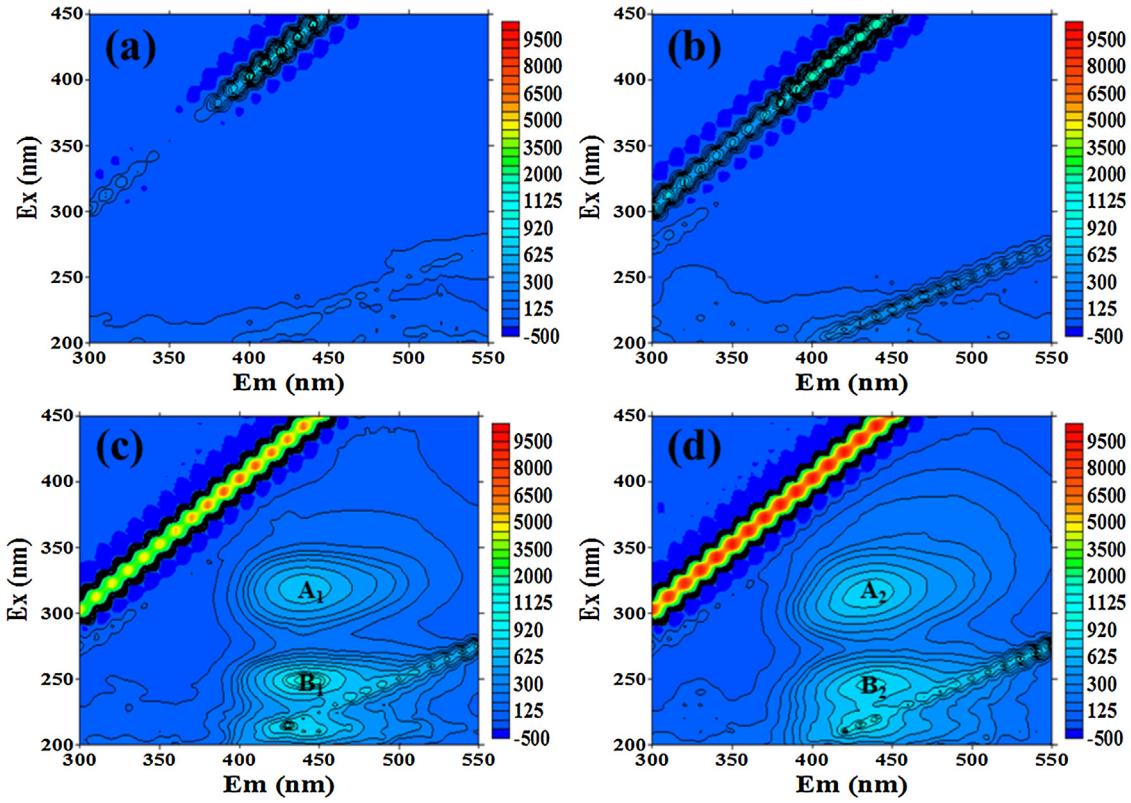

Fig. 10. 3D EEMs of (a) M1, (b) M2, (c) M3 and (d) M4.

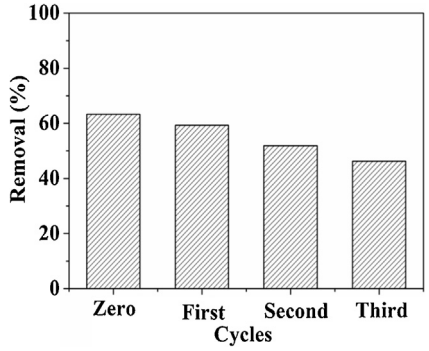

Fig. 11. Recycling tests of MLS-1 photocatalytic adsorbent under visible light irradiation.

It is suggested that MLS-1 displaying high adsorption capacity combined with efficient visible photocatalytic degradation, is favourable for the purification of TC-contaminated wastewater.

4. Conclusion

A novel core–shell In_2S_3@MIL-125(Ti) photocatalytic adsorbent with large surface area and mesoporous structure was successfully synthesized by a facile solvothermal method. The integrated photocatalytic adsorbent exhibited high adsorption affinity combined with superior photocatalytic activity for the removal of TC. The TC adsorption onto MLS was mainly ascribed to surface complexation, π–π interactions, hydrogen bonding and electrostatic interactions. It was also strongly dependent on solution pH, initial TC concentration and ion strength. The adsorption processes can be described via Langmuir isotherms and pseudo-second-order mode. Further, the TC degradation experiments under visible light irradiation showed that the additive content of optimal MIL-125(Ti) in synthesis process was determined to be 0.1 g, and the corresponding photodegradation efficiency for TC was 63.3%, which was higher than that of pure In_2S_3 and pure MIL-125(Ti), respectively. The opened porous structure, effective transfer of photo-generated carriers, Ti^{3+}–Ti^{4+} intervalence electron transfer and the synergistic effect between MIL-125(Ti) and In_2S_3 were the main reasons for improved photo-degradation performance. Most importantly, MLS-1 can efficiently remove TC from medical wastewater, municipal wastewater and river water. Therefore, it could be concluded that the novel core–shell structured materials could be used as promising integrated photocatalytic adsorbent for the purification of antibiotics from wastewater. However, since the performance of MOFs can be readily tuned by changing the constituent metal ions and bridging organic linkers, more MOFs-based photocatalytic adsorbent with various morphology and structure will be expected for the applications of environmental remediation.

Acknowledgments

The authors gratefully acknowledge the financial support provided by National Natural Science Foundation of China (Nos. 51521006, 71431006, 71221061) and Shanghai Tongji Gao Tingyao Environmental Science and Technology Development Foundation.

Appendix A. Supplementary data

Supplementary data associated with this article can be found, in the online version, at http://dx.doi.org/10.1016/j.apcatb.2015.12.041.

References

[1] G. Zeng, M. Chen, Z. Zeng, Science 340 (2013) 1403.
[2] B. Petrie, R. Barden, B. Kasprzyk-Hordern, Water Res. 72 (2015) 3–27.

[3] S. Reardon, Nautre 509 (2014) 141–142.
[4] S. Rodriguez-Mozaz, S. Chamorro, E. Marti, B. Huerta, M. Gros, A. Sanchez-Melsio, C.M.V. Borrego, D. Barcelo, J.L. Balcazar, Water Res. 69 (2015) 234–242.
[5] Z. Cetecioglu, B. Ince, M. Gros, S. Rodriguez-Mozaz, D. Barceló, D. Orhon, O. Ince, Water Res. 47 (2013) 2959–2969.
[6] I. Michaela, L. Rizzob, C.S. McArdellc, C.M. Manaiad, C. Merline, T. Schwartzf, C. Dagotg, D. Fatta-Kassinosa, Water Res. 47 (2013) 957–995.
[7] H. Wang, X. Yuan, Y. Wu, H. Huang, X. Peng, G. Zeng, H. Zhong, J. Liang, M. Ren, Adv. Colloid Interface Sci. 195–196 (2013) 19–40.
[8] H. Jing, T. Wen, C. Fan, G. Gao, S. Zhong, A. Xu, J. Mater. Chem. A 2 (2014) 14563–14570.
[9] K. Baransi, Y. Dubowski, I. Sabbah, Water Res. 46 (2012) 789–798.
[10] I. El Saliby, L. Erdei, J.H. Kim, H.K. Shon, Water Res. 47 (2013) 4115–4125.
[11] H. Dong, G. Zeng, L. Tang, C. Fan, C. Zhang, X. He, Y. He, Water Res. 79 (2015) 128–146.
[12] H. Furukawa, K.E. Cordova, M. O'Keeffe, O.M. Yaghi, Science 341 (2013) 1230444.
[13] E. Barea, C. Montoro, J.A.R. Navarro, Chem. Soc. Rev. 43 (2014) 5419–5430.
[14] Y. Peng, Y.S. Li, Y.J. Ban, H. Jin, W.M. Jiao, X.L. Liu, W.S. Yang, Science 346 (2014) 1356–1359.
[15] B. Van de Voorde, B. Bueken, J. Denayer, D. De Vos, Chem. Soc. Rev. 43 (2014) 5766–5788.
[16] T. Zhang, W. Lin, Chem. Soc. Rev. 43 (2014) 5982–5993.
[17] S. Vaesen, V. Guillerm, Q. Yang, A.D. Wiersum, B. Marszalek, B. Gil, A. Vimont, M. Daturi, T. Devic, P.L. Llewellyn, C. Serre, G. Maurin, G.D. Weireld, Chem. Commun. 49 (2013) 10082–10084.
[18] H. Guo, F. Lin, J. Chen, F. Li, W. Weng, Appl. Organomet. Chem. 29 (2015) 12–19.
[19] M. Dan-Hardi, C. Serre, T. Frot, L. Rozes, G. Maurin, C. Sanchez, G. Férey, J. Am. Chem. Soc. 131 (2009) 10857–10859.
[20] H. Wang, X. Yuan, Y. Wu, G. Zeng, X. Chen, L. Leng, Z. Wu, L. Jiang, H. Li, J. Hazard. Mater. 286 (2015) 187–194.
[21] H. Wang, X. Yuan, Y. Wu, G. Zeng, X. Chen, L. Leng, H. Li, Appl. Catal. B: Environ. 174–175 (2015) 445–454.
[22] H. Wang, X. Yuan, Y. Wu, X. Chen, L. Leng, G. Zeng, RSC Adv. 5 (2015) 32531–32535.
[23] X. An, J.C. Yu, F. Wang, C. Li, Y. Li, Appl. Catal. B: Environ. 129 (2013) 80–88.
[24] C. Wei, W. Guo, J. Yang, H. Fan, J. Zhang, W. Zheng, RSC Adv. 4 (2014) 50456–50463.
[25] J. Zhou, G. Tian, Y. Chen, Y. Shi, C. Tian, K. Pan, H. Fu, Sci. Rep. 4 (2014) 4027.
[26] X. Zhang, X. Li, C. Shao, J. Li, M. Zhang, P. Zhang, K. Wang, N. Lu, Y. Liu, J. Hazard. Mater. 260 (2013) 892–900.
[27] Z. Wu, H. Zhong, X. Yuan, H. Wang, L. Wang, X. Chen, G. Zeng, Y. Wu, Water Res. 67 (2014) 330–344.
[28] Y. Shi, S. Xing, X. Wang, S. Wang, Bioresour. Technol. 139 (2013) 170–175.
[29] S. Valencia, J.M. Marin, G. Restrepo, F.H. Frimmel, Water Res. 51 (2014) 124–133.
[30] H. Wang, X. Yuan, G. Zeng, L. Leng, X. Peng, K. Liao, L. Peng, Z. Xiao, Environ. Sci. Pollut. Res. Int. 21 (2014) 11552–11564.
[31] X. Fu, X. Wang, Z. Chen, Z. Zhang, Z. Li, D.Y.C. Leung, L. Wu, X. Fu, Appl. Catal. B: Environ. 95 (2010) 393–399.
[32] M.R. Bayati, A.Z. Moshfegh, F. Golestani-Fard, Appl. Catal. A: Gen. 389 (2010) 60–67.
[33] Z. Hasan, S.H. Jhung, J. Hazard. Mater. 283 (2015) 329–339.
[34] Y. Zhao, X. Gu, S. Gao, J. Geng, X. Wang, Geoderma 183–184 (2012) 12–18.
[35] L. Duan, L. Li, Z. Xu, W. Chen, Environ. Sci. Process. Impacts 16 (2014) 1462–1468.
[36] F. Yu, J. Ma, S. Han, Sci. Rep. 4 (2014) 5326.
[37] Y. Ma, Q. Zhou, S. Zhou, W. Wang, J. Jin, J. Xie, A. Li, C. Shuang, Chem. Eng. J. 258 (2014) 26–33.
[38] K.R. Hall, L.C. Eagleton, A. Acrivos, T. Vermeulen, Ind. Eng. Chem. Res. 5 (1966) 212–223.
[39] Y.H. Fu, D.R. Sun, Y.J. Chen, R.K. Huang, Z.X. Ding, X.Z. Fu, Z.H. Li, Angew. Chem. Int. Ed. Engl. 51 (2012) 3364–3367.
[40] J. Gao, J. Miao, P. Li, W.Y. Teng, L. Yang, Y. Zhao, B. Liu, Q. Zhang, Chem. Commun. 50 (2014) 3786–3788.
[41] C.C. Wang, J.R. Li, X.L. Lv, Y.Q. Zhang, G. Guo, Energy Environ. Sci. 7 (2014) 2831–2867.
[42] C. Song, X.F. Sun, S.F. Xing, P.F. Xia, Y.J. Shi, S.G. Wang, Environ. Sci. Pollut. Res. Int. 21 (2014) 1786–1795.
[43] P.G. Coble, Mar. Chem. 51 (1996) 325–346.